

Limiter observations during W7-X first plasmas

This content has been downloaded from IOPscience. Please scroll down to see the full text.

2017 Nucl. Fusion 57 056036

(<http://iopscience.iop.org/0029-5515/57/5/056036>)

View [the table of contents for this issue](#), or go to the [journal homepage](#) for more

Download details:

IP Address: 192.167.140.72

This content was downloaded on 15/05/2017 at 15:25

Please note that [terms and conditions apply](#).

You may also be interested in:

[Plans for the first plasma operation of Wendelstein 7-X](#)

T. Sunn Pedersen, T. Andreeva, H.-S. Bosch et al.

[Thermographic study of heat load asymmetries during MAST L-mode discharges](#)

G De Temmerman, E Delchambre, J Dowling et al.

[Numerical investigation of plasma edge transport and limiter heat fluxes in Wendelstein 7-X startup plasmas with EMC3-EIRENE](#)

F. Effenberg, Y. Feng, O. Schmitz et al.

[Plasma boundary phenomena in tokamaks](#)

P.C. Stangeby and G.M. McCracken

[JET MKII Gas-Box ELM energy distribution](#)

T Eich, P Andrew, A Herrmann et al.

[Scrape-off layer properties of ITER-like limiter start-up plasmas in JET](#)

G. Arnoux, T. Farley, C. Silva et al.

[Divertor program in stellarators](#)

R König, P Grigull, K McCormick et al.

[Diagnostic set-up and modelling for investigation of synergy between 3D edge physics and plasma-wall interactions on Wendelstein 7-X](#)

Y. Liang, O. Neubauer, R. König et al.

Limiter observations during W7-X first plasmas

G.A. Wurden¹, C. Biedermann², F. Effenberg³, M. Jakubowski^{2,4},
H. Niemann², L. Stephey³, S. Bozhenkov², S. Brezinsek⁵, J. Fellinger²,
B. Cannas⁶, F. Pisano⁶, S. Marsen², H.P. Laqua², R. König², O. Schmitz³,
J.H. Harris⁷, E.A. Unterberg⁷ and the W7-X Team²

¹ Los Alamos National Laboratory, PO Box 1663, Los Alamos, NM 87545, United States of America

² Max Planck Institut für Plasmaphysik, Wendelsteinstr. 1, 17491 Greifswald, Germany

³ University of Wisconsin, Madison, WI 53706, United States of America

⁴ University of Szczecin, Institute of Physics, 70-451 Szczecin, Poland

⁵ Forschungszentrum Jülich GmbH, IEK-4 52425 Jülich, Germany

⁶ University of Cagliari, Via Università 40, 09124 Cagliari, Italy

⁷ Oak Ridge National Laboratory, PO Box 2008, Oak Ridge, TN 37831, United States of America

E-mail: wurden@lanl.gov

Received 15 December 2016, revised 7 March 2017

Accepted for publication 10 March 2017


Published 3 April 2017



Abstract

During the first operational phase (referred to as OP1.1) of the new Wendelstein 7-X (W7-X) stellarator, five poloidal graphite limiters were mounted on the inboard side of the vacuum vessel, one in each of the five toroidal modules which form the W7-X vacuum vessel. Each limiter consisted of nine specially shaped graphite tiles, designed to conform to the last closed field line geometry in the bean-shaped section of the standard OP1.1 magnetic field configuration (Sunn Pedersen *et al* 2015 *Nucl. Fusion* **55** 126001). We observed the limiters with multiple infrared and visible camera systems, as well as filtered photomultipliers. Power loads are calculated from infrared (IR) temperature measurements using THEODOR, and heating patterns (dual stripes) compare well with field line mapping and EMC3-EIRENE predictions. While the poloidal symmetry of the heat loads was excellent, the toroidal heating pattern showed up to a factor of $2\times$ variation, with peak heat loads on Limiter 1. The total power intercepted by the limiters was up to $\sim 60\%$ of the input ECRH heating power. Calorimetry using bulk tile heating (measured via post-shot IR thermography) on Limiter 3 showed a difference between short high power discharges, and longer lower power ones, with regards to the fraction of energy deposited on the limiters. Finally, fast heating transients, with frequency > 1 kHz were detected, and their visibility was enhanced by the presence of surface coatings which developed on the limiters by the end of the campaign.


Keywords: W7-X, stellarator, infrared, heat loads, limiter

 Supplementary material for this article is available [online](#)

1. Introduction

During the first operational phase (OP1.1) of the new W7-X stellarator, specially shaped poloidal graphite limiters, each consisting of nine discrete tiles, served as the main plasma facing

component, with one limiter per module [1, 2]. They were located on the inboard side of the modules at the bean-shaped plasma cross-section. Measuring the power fluxes to these limiters was essential, both from an engineering and scientific viewpoint. Because the machine had a large surface area of exposed copper tiles, and also no plasma exposed water-cooled components (yet), it was important to know that most of the power was either going to the 5 graphite limiters, or that it was being radiated away to the entire vessel. Since we didn't want to melt unprotected elements,

 Original Content from this work may be used under the terms of the [Creative Commons Attribution 3.0 licence](#). Any further distribution of this work must maintain attribution to the author(s) and the title of the work, journal citation and DOI.

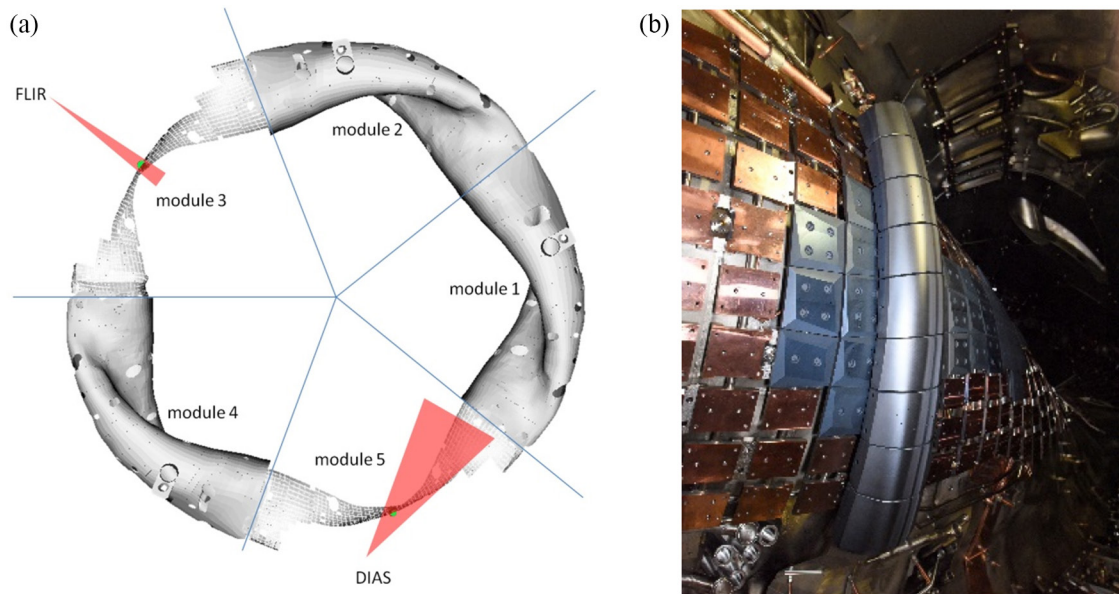


Figure 1. (a) A top-down CAD view of the W7-X inner vessel, showing sightlines of the radially viewing FLIR and toroidally viewing DIAS IR camera systems, with cutaway in module 3 and 5, respectively. At this scale, the limiters are small green blobs. (b) Side view photo of Limiter 5, showing the nine graphite tiles (we number them 1 through 9, from top to bottom) which make up each limiter. Most of the copper mounting blocks (also visible) were not covered with graphite during OP1.1.

there was initially a (very conservative) 2 MJ administrative maximum limit for the energy input in any one discharge. During the course of the campaign, also a result of our measurements, this was increased to 4 MJ. Infrared camera systems are used in magnetic fusion experiments, world-wide, to measure heat loads on vessel components [3–6]. Due to the helical symmetry with five modules in W7-X, there will eventually be on the order of 10–20 camera systems (2 or more IR cameras viewing in each module) to cover the entire vessel for long pulse operation, all with real-time analysis and large data streams. But for OP1.1, we started with a more basic diagnostic set.

2. Methods

A top-down schematic of our IR camera views is shown in figure 1(a), showing cutaway of the vessel in two modules, with the IR sightlines in red, and the projection of two of the limiters in green. A photo looking inwards towards limiter in Module 5 is shown in figure 1(b).

We used a variety of instruments to monitor the status of the five limiters, including a dedicated set of diagnostics to observe their performance and infer basic transport behaviour of the 3D helical SOL plasma. In addition to a set of low resolution near-IR cameras [7], we had a 3–5 μm band infrared (FLIR SC8303HD) camera (125 Hz full-frame rate, 1344×768 pixels) and a 400–800 nm AVT Prosilica GX-1050C (100 Hz full-frame rate, 1024×1024 pixels) color visible camera co-located on the same line of sight in Module 3 [8]. Additionally, an 8–14 μm DIAS IR camera (50 Hz, 640×480 pixels) viewed one side of Limiter 5 [9]. Near-IR cameras viewed Limiters 1 and 5 from the ECRH launcher positions [1]. A 24-channel filterscope, consisting of filtered photomultipliers fed by fiber-optics, has been used for first measurements at W7-X [10]. Spatial channels at five different port locations were split into four spectral

channels each—C-II (515 nm), H-beta (486 nm), He-I (667 nm), and H-alpha (656 nm). For future reference, we note that the H-alpha filter used was susceptible to possible spectral contamination from C-II at 657.8 nm. Each viewing chord has a width of approximately 2.5 cm, although the one at Limiter 3 had a 16 cm diameter (to match the width of the limiter). This gives us simultaneous visible and IR imagery to go along with time-resolved filtered light traces, along the same lines of sight. Taken together, these instruments enabled us to develop information on edge plasma and wall conditions, and provided input for edge plasma codes to enable a beginning of our understanding of the plasma wall interactions in the W7-X stellarator.

3. Results

This paper focuses on high resolution infrared observations which enabled heat flux and power load measurements on the limiters. We describe general features of the limiter observations, using the FLIR IR camera as a limiter calorimeter, time-resolved power flux calculations, asymmetries seen on the limiters, first observations of transient features on the limiters, comparisons to numerical field line/power load modeling, and finally surface feature changes on the limiters which evolved during the campaign.

3.1. General features

The first helium plasmas (in Dec 2015), were small in diameter and highly radiating, and consequently the limiters initially received little deposited energy (only a few $^{\circ}\text{C}$ surface temperature increase). In fact, in the very first plasma (a helium discharge), an ECRH resonance filament of cold dense plasma with a diffuse outer region, nicely illuminated the field line directions in front (and above) the tiles on Limiter 3, as seen in the true color image in figure 2(a).

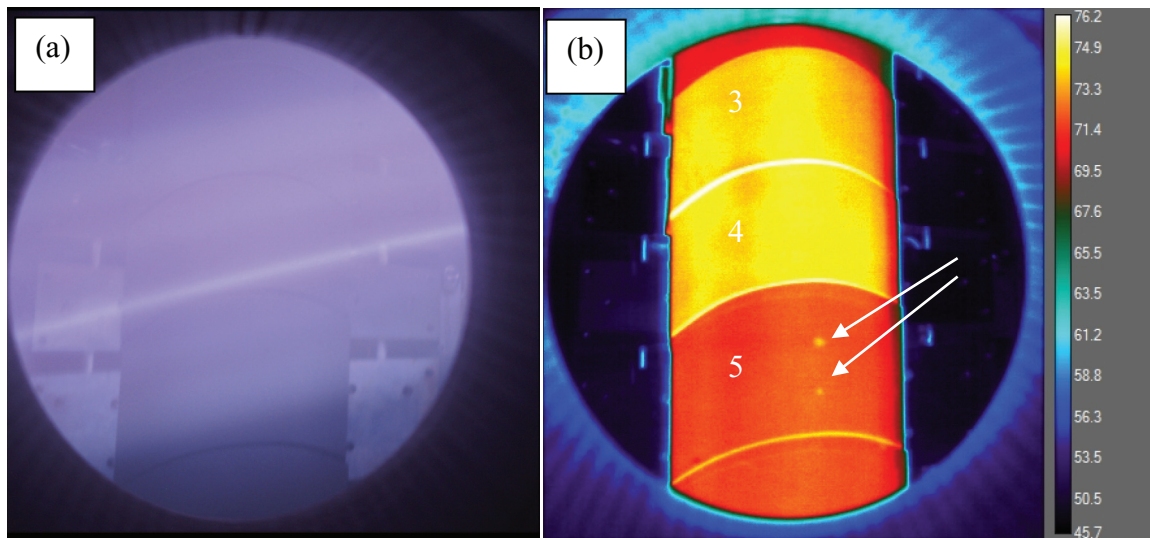


Figure 2. (a) True color image of the first helium discharge in W7-X (Dec. 10, 2015), with bright filament (region of strong ECRH absorption) showing the local magnetic field line angle above the limiter mid-plane on Limiter 3. (b) Same view of Limiter 3, but apparent temperature seen with the FLIR IR camera, showing limiter tiles at slightly different temperatures between discharges. Tiles 3–5 are seen in their entirety. Defect spots on tile 5 are indicated by arrows.

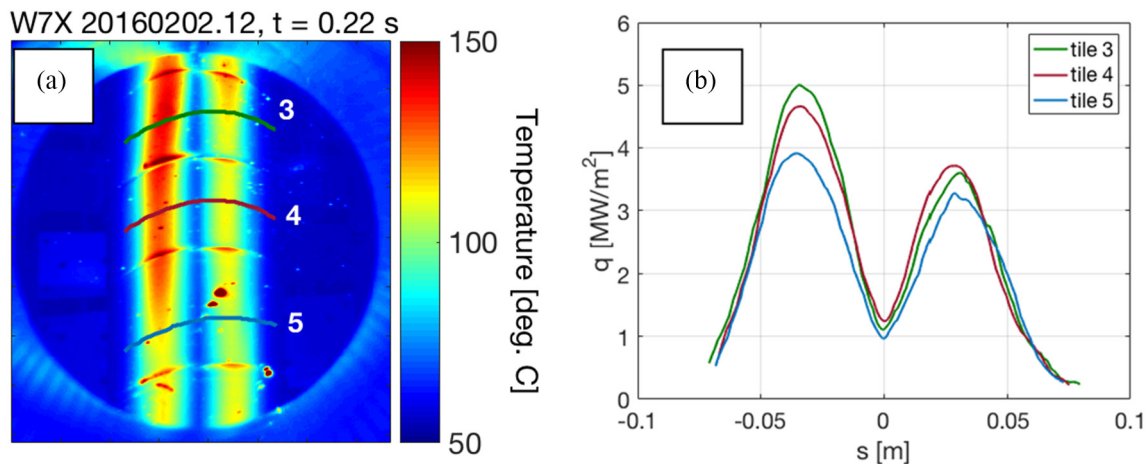


Figure 3. (a) Typical dual-stripe IR heating pattern seen on the Limiter 3 central tiles (20160202.012). (b) Resulting heat flux profiles (away from leading edge effects) along curved surface coordinates (green, red, blue lineout overlay) across tiles 3–5, respectively.

The FLIR IR camera (located in the AEA30 port, viewing radially inwards and upwards from 60° below the mid-plane [8]) could see all or part of five of the nine tiles of Limiter 3 (figure 2(b)). Due to poor thermal contact and long cooling times between shots, the tiles would equilibrate with themselves, before giving much of their heat to the cooled vessel wall, or to each other.

In Jan. 2016, plasmas improved as the walls were conditioned with helium glow discharge cleaning (prior to energizing the superconducting coils). But because we could not glow discharge between shots during the day (the magnetic fields are steady-state), we conducted a repetitive series of helium pulsed discharge conditioning plasmas (one megawatt 50 ms ECRH (electron cyclotron resonance heating) pulse every 30 s, ten times in a row, to warm the walls, while allowing time for pump-out of out-gassed materials between pulses) followed by the ‘real’ main pulse. We define a main pulse as one with full diagnostics, and part of the physics

program. Discharges grew in diameter (to fully contact the limiters), in pulse length (up to 6 s), in power and input energy (up to 4 MW and 4 Megajoules).

Dual contact stripes on the limiter surface became the dominant infrared feature, as shown in figure 3(a), for a 3.7 MW discharge. The stripes have a separation of 5.5–6 cm, and a FWHM (full width half maximum) distance of 4–4.5 cm (which is important for later visual comparison of the erosion/deposition patterns). We show a single time slice of the heat flux profiles in figure 3(b), generated using the FLIR IR camera temperature input data in the thermal analysis code THEODOR [11, 12]. We note that in our range of temperatures, it was especially important to include temperature dependent thermal properties of the high-density graphite in THEODOR.

During a pulse, the tile surface temperatures increased as the square root of time during shots with constant heating power, as expected from energy impinging on un-cooled ‘semi-infinite’ solids. As predicted [1, 2, 15], the highest

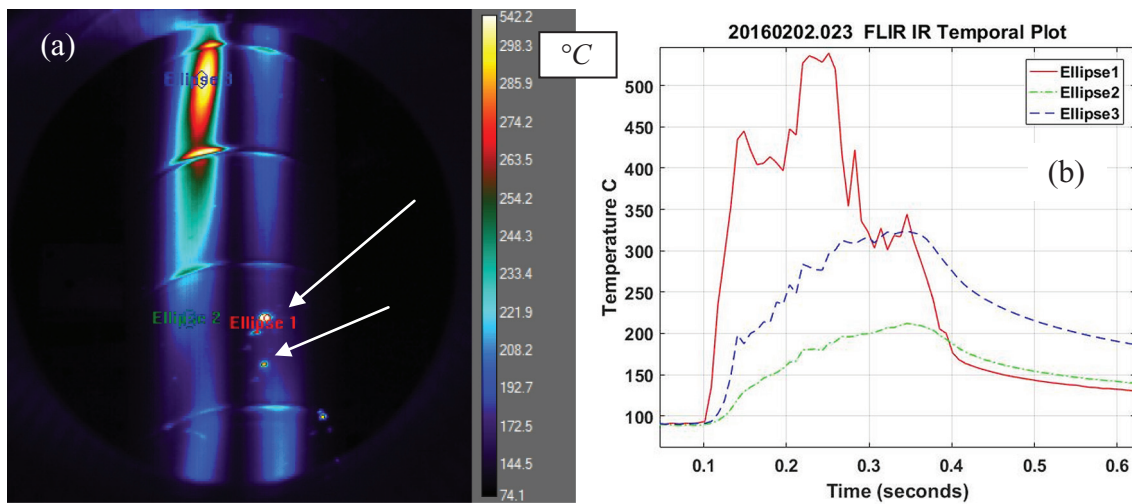


Figure 4. Shot 20160202.023, a 4 MW short pulse helium plasma. (a). Limiter 3 infrared temperature image. Several defect hot spots (arrows), >500 °C, can be seen on the right-side power stripe (b). Poor thermal contact compared to bulk tile regions (green and blue traces) is evidenced by the rapid rise /fall time history (red trace) of a hot defect spot in the time-history plot, compared to two other (bulk) regions.

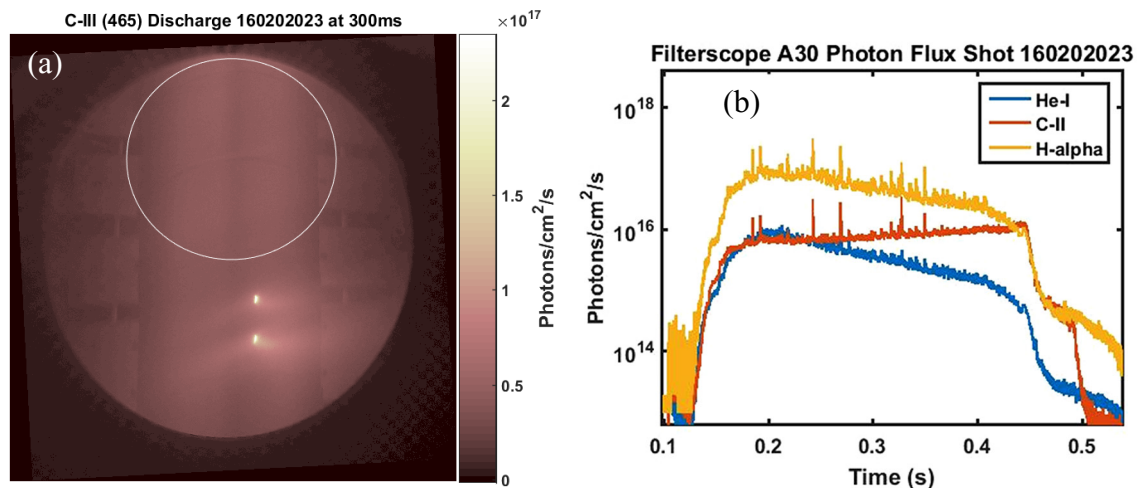


Figure 5. Shot 201600202.023 (continued) (a). Two carbon blooms in CIII light (465 nm) on tile 5, limiter 3. (b). Filtered photomultiplier time traces looking directly at the Module 3 limiter (white circle), showing some fluctuation, but missing the carbon blooms.

points or ‘watershed’ of the curved limiters between the two heating stripes did not intercept much energy. This is because at the peak of the limiter curved surface, the field lines are nearly tangential, whereas further down on the side of the curved limiter, the field lines intercept the limiter at a large angle. Since the parallel heat flux is much higher than the perpendicular heat flux, the maximum heat flux density is shifted outside the last closed flux surface. Also, the lower leading edge on the left side of each tile, and the upper edge on the right side of each tile received the highest heat fluxes, a pattern consistent with particle transport along the magnetic field lines.

Sometimes carbon blooming behaviour could be seen, in addition to the power stripes, as shown for example in figures 4 and 5, during shot 20160202.023, which used 6 ECRH gyrotrons, with a total of just less than 4 MW of input power.

On Limiter 3, tile 5, there were two hot spots (>500 °C) (figure 4(a)), which showed real carbon bloom behaviour, even including hot material (tiny flying dusts (UFO’s) seen in the FLIR IR video images) flying from them. Time histories of the three labelled ellipse locations in figure 4(a) are also shown in figure 4(b). Simultaneously, there was bright, localized emission in CIII light, as observed with the Prosilica visible camera (see figure 5(a)). These imperfection locations were present in pre-run visible light images, and behaved as if they had reduced thermal contact to the bulk material. Even though filtered line emission measurements looked directly at the limiter with good temporal resolution (100kHz) (see figure 5(b)), and were used to determine neutral and impurity densities and particle fluxes [13], in this case we know the filterscope sightline did not include the carbon bloom locations. A further issue was that the 2.5 nm bandwidth interference

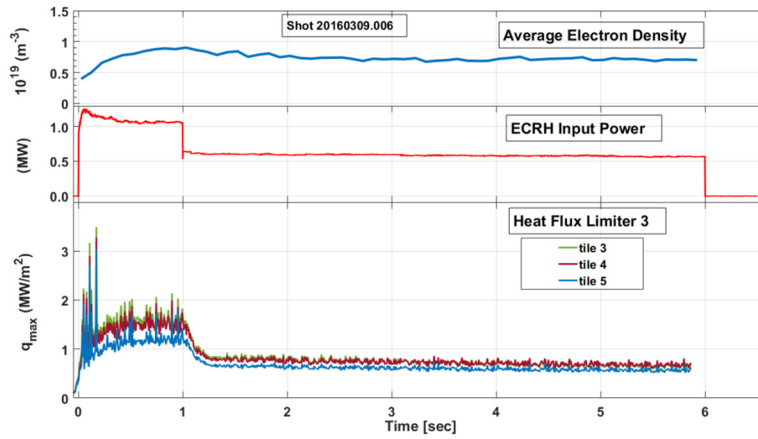


Figure 6. Averaged electron density, ECRH power, and maximum power flux on the left-side heat stripe (Limiter 3) calculated with data for tiles 3, 4, and 5, from IR thermography images over time using THEODOR, for a long duration low power discharge.

Table 1. Energy absorbed by Limiter 3 during a 6 s, 4 MJ discharge (20160309.006). Quantities in parenthesis are estimated by symmetry, and information from the Limiter 5 (full length) IR view.

Tile	C_p (kJ °C ⁻¹)	ΔT_c (°C)	E (kJ)	$\pm \Delta E$ (kJ)
1	1.49	(28)	(42)	6
2	1.21	32.6	39.4	1
3	1.13	35.4	40.0	1
4	1.05	37.6	39.5	1
5	1.25	35.1	43.9	1
6	1.05	34.1	35.8	1
7	1.13	(35.4)	(40.0)	4
8	1.21	(32.6)	(39.4)	4
9	1.49	(28)	(42)	6
Sum			362	± 25

filters were used, and in the case of H-alpha, there is a nearby competing C-II line at 657.8 nm, which could cause spectral pollution. This pre-puff filled helium discharge, in addition to helium, also clearly had significant hydrogen present as well.

3.2. IR calorimetry

The high resolution FLIR camera could resolve 10 milli-Kelvin temperature differences, so it was useful to make calorimetry measurements of bulk tile temperature changes, due to the integrated energy deposited, on a shot-by-shot basis. The IR camera measures a surface temperature during the shot, but by several minutes after a shot (in particular, immediately before the next pulse begins) it transitions into a bulk temperature. Individual tiles are well-insulated thermally from each other, so we can record six different bulk temperature readings, one for each of tiles 2 through 6 in the camera field of view on Limiter 3. By observing the decay rate of the bulk tile temperature (-6 °C/1000s at the end of the day) through the mounting brackets to the vessel wall, we can extrapolate backwards from the bulk tile temperature observed a few minutes after the shot, to what it would have been immediately at the end of the previous shot, and infer the temperature change (ΔT_c) caused by that shot. Therefore, taking into account the

tile heat capacities (C_p), we could directly measure the energy absorbed by each tile. While we could only see five of the nine tiles on Limiter 3, we also had poloidal symmetry information from Limiter 5, where we could see the entire length of one side of the limiter (shown later for example in figure 7(b)). The up-down plasma contact on the limiters was, to first approximation, quite uniform [9]. Table 1 shows an example calculation of the energy absorbed by Limiter 3, during a 6 s shot (20160309.006) with ECRH input energy of 1 MW for 1 s and 0.6 MW for 5 s (total of 4 MJ energy). Later (section 3.4) we will show how to convert this single-limiter absorbed energy, into the total energy deposited on all five limiters. For this discharge, during the low-power phase, the line averaged electron density was 7×10^{12} cm⁻³, central electron temperature was 6 keV, and central ion temperature was 1.7 keV, while the bolometer observed $\sim 30\%$ of the energy as plasma radiation.

3.3. Power fluxes

As noted previously, time history of limiter power fluxes were calculated using IR surface temperature input data as a function of time, using an improved THEODOR code utilizing temperature-dependent thermal properties of the high-density graphite tiles. Continuing to use our ‘typical’ 6 s shot, examples of the peak power flux on three tiles of Limiter 3 are shown in figure 6. The camera unfortunately wasn’t set to acquire data for the entire pulse, hence the final 1/2 s or so is missing on the IR trace. For 4 MW discharges, heat fluxes were ~ 5 MW m⁻² (as shown previously in figure 3). For this discharge, the electron density is obtained by averaging the Thomson scattering density profiles, at a 10 Hz repetition rate.

We find that when comparing the local time-resolved power flux measurements to the time/surface integrated calorimetry measurement, each technique has advantages and disadvantages. For the calorimetry measurement, there is no issue with integrating the power flux over the area on the limiter, because the heat spreads out into the whole tile independently of the deposition area. While converting the observed power fluxes to energy absorbed, one must carefully integrate over the appropriate area(s) on the limiter, as well as over time in

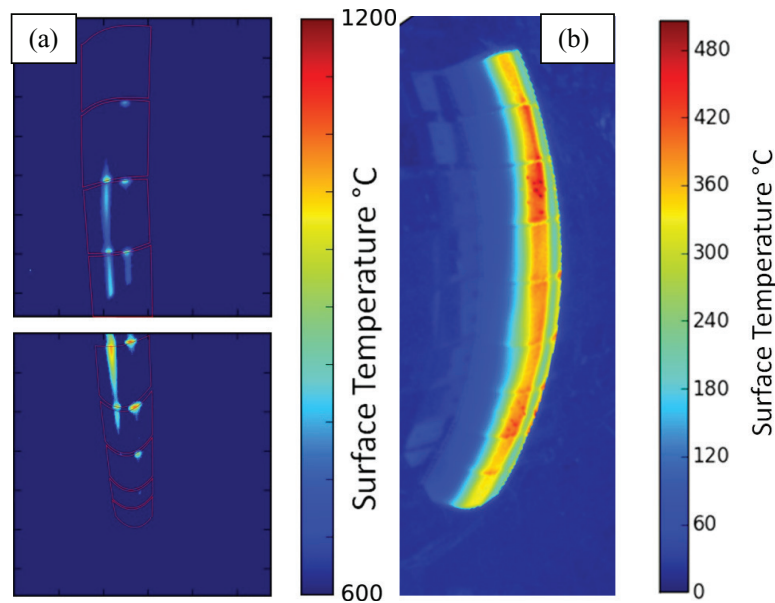


Figure 7. We were surprised to measure temperatures over $1000\text{ }^{\circ}\text{C}$ on Limiter 1, when all other Limiters were cooler. Shot 20160310.009 (a) on the left is split-view example image (immediately post-shot) from a near-IR camera viewing Limiter 1 from the outside port at the ECRH launcher location in Module 1. The tiles are outlined in red. (b) By comparison, at the end of the same discharge, the side viewing DIAS long-wavelength camera shows neighboring Limiter 5 to be less than $500\text{ }^{\circ}\text{C}$. (The hot dots on tiles 3 and 7 are due to the Langmuir probe arrays).

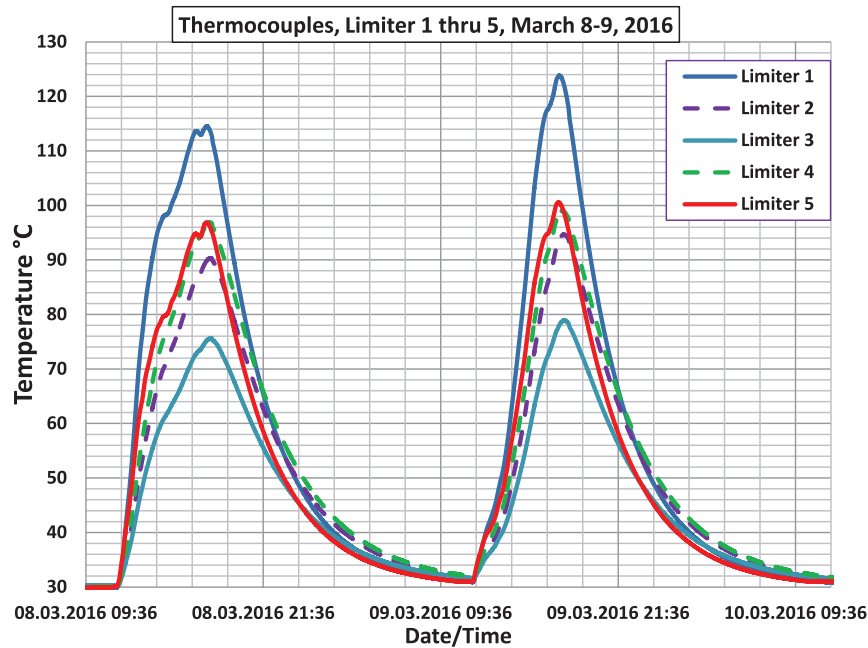


Figure 8. Data from slow thermocouples mounted on a bracket behind tile 2 for each of the five limiters, integrating over 2 d of operation. Limiter 3 saw consistently less heating (energy) than Limiter 1.

the discharge. The problem is that no single diagnostic sees the whole limiter. On the other hand, a comparison of the total absorbed energy measurement to the known ECRH input energy, is affected both by the startup time ($\sim 100\text{ ms}$ when the plasma is too small to contact the limiter) and by the shutdown time ($\sim 100\text{--}200\text{ ms}$ where when a radiative collapse occurs, the energy doesn't go to the limiter, but instead to the entire vessel). So the two techniques differ more for short duration discharges than for longer ones. Consequently we view the two measurements as complementary.

3.4. Asymmetries

The near-IR camera on Limiter 1 saw much higher temperatures ($\sim 1000\text{ }^{\circ}\text{C}$) on high energy discharges than our systems viewing Limiters 3 or 5. An example of this data (Shot 20160310.009, a 4 MW, 1.2 s long pulse) is shown in figure 7. However this system could not resolve temperatures below $600\text{ }^{\circ}\text{C}$, as the near-IR views suffered from plasma light contamination during a pulse. Therefore we could only get data from the near-IR views some 100 ms or so after a shot, when



Figure 9. The five limiters from W7-X OP1.1, laid out in the laboratory after the run. Dual erosion/deposition stripes are noteworthy, and are remarkably similar on limiters 2–5, but differ strongly on the middle tiles of limiter 1 where the stripes fade away. There is a small top/bottom asymmetry in the stripe pattern on all five limiters. (The golden hue on some tiles is real, and is an interference film effect which is strongly dependent on the camera viewing angle).

the plasma light was gone. Interestingly, a second near-IR system in Module 5, viewing Limiter 5, never saw any useful signals, indicating temperatures there were always less than 600 °C, which was consistent with what the long-wavelength DIAS camera at the same limiter also reported, as shown in figure 7(b). The DIAS camera gave very nice IR images of one side of the entire length of Limiter 5.

Consequently, we knew there were toroidal asymmetries on the limiter power loads. Fortunately, we had another system...albeit a very slow one...that provided confirming data from each limiter. There were a set of 10 thermocouples, (two per limiter), mounted between the limiter tiles and the cooled vessel wall. These slow thermocouples in the back of the limiter mounting brackets provided additional toroidal symmetry information (data from the upper ones on each limiter are shown in figure 8), indicating Limiter 1 was hotter by a factor of 1.9× than Limiter 3, and that Limiters 2, 4, and 5 were similar to each other. Overall, a multiplier of 7× times the power/energy incident on Limiter 3 (rather than 5× if fully symmetric), is our best estimate for the power/energy which flowed to the limiters. As a result, in the previous example (shot 20160309.006), we calculate that 2.5 MJ went to the limiters, or $62 \pm 10\%$ of the microwave input energy. But using the same methodology, high-power (4 MW), 1 s shots

had only ~35–45% of the energy going to the limiters, while at the same time the bolometers could account for an additional ~25–40% as radiation. As a result, the unaccounted fractional energy loss is higher in the high power discharges [14].

Post-run limiter inspection also revealed that the plasma interaction with Limiter 1 was qualitatively different, in the observed erosion/deposition pattern, compared to all of the other four limiters. In particular, the dark stripe pattern was surprisingly weak on the middle tiles of Limiter 1. This can be seen in figure 9, where all five limiters are photographed side-by-side in the laboratory. We now realize that this ‘weakness’ of the burn stripe, is because it is more eroded in this area (compared to the other limiters). This difference is another piece of evidence that Limiter 1 had a more intense plasma interaction when compared to the other limiters. As a further note for the reader, the holes on tiles 3 and 7, Limiter 5, were where the Langmuir probe arrays were located.

In addition to the observed toroidal asymmetry noted above, post run visual examination of each limiter also revealed that at the bottom of the limiters, the erosion pattern extended straight off the bottom tile (#9), whereas at the top of the limiter (on tile #1), the pattern did not reach the end of the tile, and furthermore it curved off slightly to the right. The power load pattern symmetry point on the central tile seen by

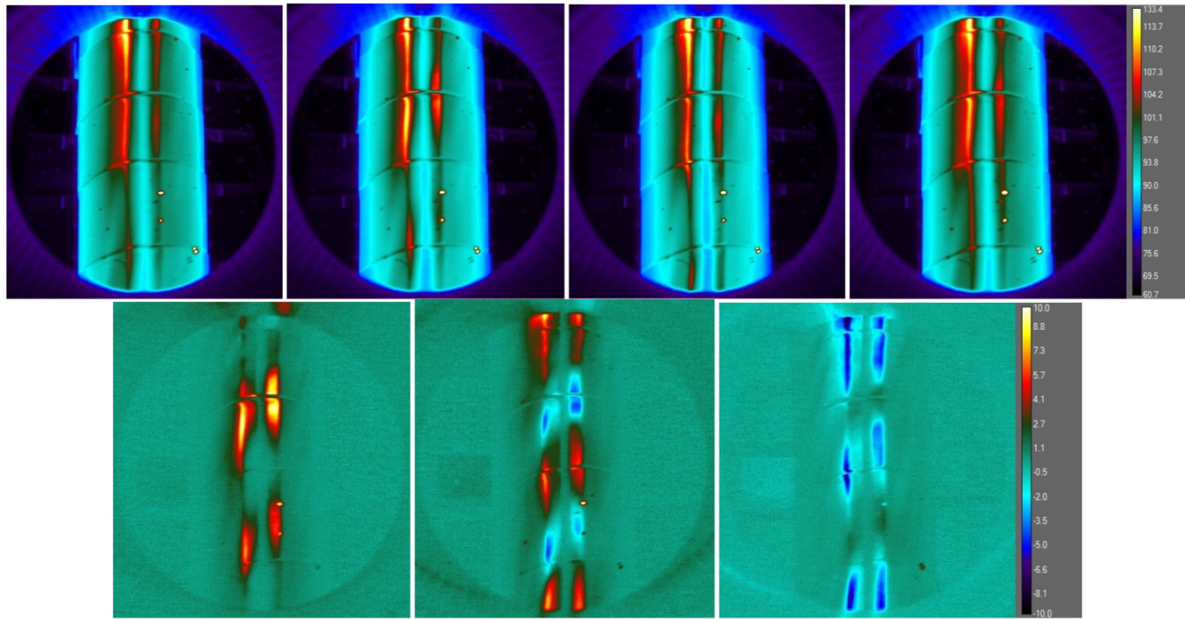


Figure 10. Using a sliding frame subtraction technique, we enhance the visibility of high frequency differential temperature (energy) bursts on shot 20160302.023. Frames 84–87 are displayed (from left to right) in the top row, and corresponding differenced frames are shown in the lower row.

the IR cameras is also low by 3–4 centimeters. We believe this could be consistent with ExB particle drifts, where (negative) radial electric fields at the plasma edge would cause an up-down asymmetry.

3.5. Transients

‘Bursty’ behavior of the limiter 3 IR emission was apparent in some discharges. Although the FLIR camera basic full frame rate is 125 Hz, we routinely ran it with a sub-frame rate of 424 Hz, with exposure times ranging from 0.5 ms down to 40 μ s. This enabled us to see faster events, but we couldn’t necessarily follow them from frame to frame. We did see indications of field-aligned filamentary transient heating bursts near, and on both sides of the watershed, at >1 kHz frequency, as shown in figure 10. The upper four frames are consecutive 0.5 ms exposures, taken at 424 Hz, with the FLIR IR camera on shot 20160302.023, at 125 ms into a 3.6 MW (1 MW of second harmonic X-mode and 2.6 MW of second harmonic O-mode ECR heating) discharge. The temperature scale spans 61 to 134 degrees Centigrade. To generate the lower three frames, sliding subtraction has been used (that is to say, each of the upper frames is differenced with respect to the preceding frame), but now the difference temperature scale spans -10 to $+10$ degrees Centigrade. A fine structure mode pattern can be seen, but the frame rate is not fast enough to distinguish movement poloidally along the limiter, if it is present.

We noticed this effect most noticeably early in time in 2–4 MW discharges. The visibility of bursts was also enhanced over the course of the last 3–4 weeks of OP1.1, by the development of surface coatings near the power stripes (which can be seen by the appearance of narrow striping in the upper four frames of figure 10). These (weakly coupled) surface layers had the effect of enhancing the visibility of fast transient

heat pulses because they could heat up and cool down more quickly than the bulk material. We are still investigating what is responsible for these events, including their fine structure.

Another form of transients involved the detection of flying dust (UFO’s) by the FLIR IR camera (across multiple frames), in about 5 % of the discharges, often in the first few shots of the morning (following helium discharge cleaning). Some were seen to originate on the graphite limiter, but others started outside of the field of view of the fast FLIR IR camera on Limiter 3, evidently from metallic regions of the vessel.

3.6. Modeling comparisons

Heat is carried to the limiters in the 3D scrape-off layer by primarily by particles carried by 3 different flux tube groups with different connection lengths: $L_c = 36$ m, 43 m, 79 m (the length depending whether you go once around the torus, or twice to the same or neighboring limiters) [2]. We show an example with IR measurements in Module 3 and direct comparisons to EMC3-EIRENE modelling in figure 11. Calculations are done for two different magnetic geometries, using 1 MW input power, a density on the last closed flux surface of 2×10^{12} cm^{-3} , and a global diffusivity of $1 \text{ m}^2 \text{ s}^{-1}$. The qualitative match between the heating stripes with the model/experiment comparison provides evidence for the expected heat and particle flux asymmetries onto the limiters, indicating a 3D helical scrape-off layer (SOL) was established. The available EMC3-EIRENE modelling results also indicate a substantial broadening of the heat flux width with increasing perpendicular transport coefficient. More calculations were done in the range of 0.5 – $2.0 \text{ m}^2 \text{ s}^{-1}$ diffusivities. We see a good match to the pattern of experimental data with global diffusivity at $\sim 1 \text{ m}^2 \text{ s}^{-1}$ [15], although EMC3-EIRENE predicts higher heat fluxes than actually observed by $\sim 2\times$. More refined estimates

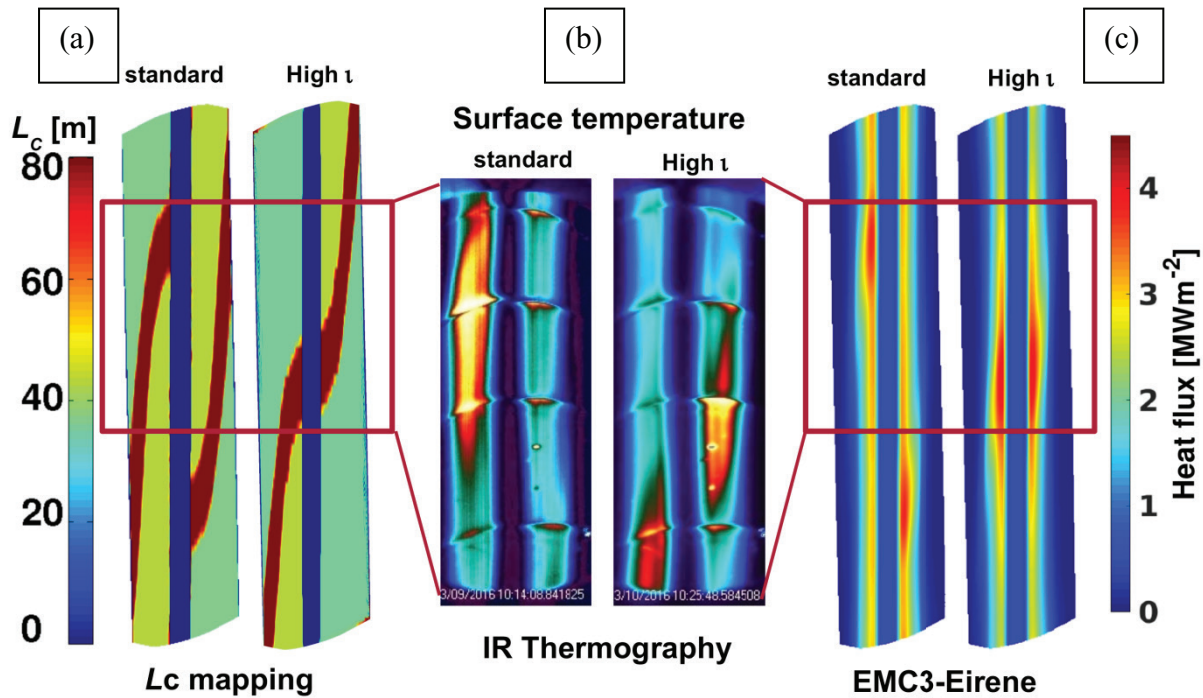


Figure 11. (a) Different length flux tubes are mapped onto the limiter surface for two magnetic configurations. (b) Infrared heating patterns (temperature from IR images) are compared with (c) EMC3-EIRENE modelling. Qualitatively, the left-right asymmetry and region of higher heating matches with the model for both standard, and higher iota discharges.

are in-progress, utilizing geodesic mapping of the curved limiter surface to scrape-off layer coordinates.

The heating pattern on the limiters in changed (as shown in figure 11(b)) when we switched to a higher iota magnetic geometry in the last 2 d of OP1.1 operation. This change in the pattern was predicted before the experiment began by EMC3-EIRENE modelling (figure 11(c)). The change was due to the different mapping of the flux tubes onto the limiter, shown in the connection length mapping depicted in figure 11(a). The basic behavior of the heating shifting from the left stripe on the top half of the limiter, to the right stripe was confirmed on multiple views. But in more detail, the code predicted a symmetric pattern on the center tile [15], while in the experiment (middle image), we see the up-down symmetry breakpoint is low by about 3–4 cm (the tiles are 16 cm wide) for both magnetic configurations. One possible reason for this shift could be because of ExB drifts, which are not included in the modelling. Also, the ‘as-built’ coil positions and deformations due to coil currents were not yet included in the magnetic configuration used for EMC3-EIRENE [15].

3.7. Surface changes

Over the course of the 3 months of operation, evidence for surface modifications of the tiles became most apparent during the latter half of the run. Inspection of the tiles after the end of OP1.1 operations was very informative. In particular, the infrared emissivity of the graphite tiles, which was nominally a uniform 0.82 before the campaign, became altered by erosion and deposition, depending on the location on the surface. Visible inspection close-up photos tiles (#3,4, & 5) from Limiter 3 are shown in figure 12(a) from directly overhead,

and at a lower angle in figure 12(b). A mid-band IR image was taken with the tile at a uniform temperature in the lab, shown in figure 12(c). The online version of this figure 12(c) shows the tile being rotated 360 degrees, to eliminate any angle-dependent viewing effects, and to show the emissivity of the unmodified back-side of the tile. Interestingly, mounting holes act very nicely as a black body, also with emissivity 1.00.

The width of the dark bands is 1.8–1.9 cm in visible light, whereas the FWHM of the temperature in each heat stripe during a shot is 4.0–4.5 cm. Surprisingly, the dark stripes (visible image) did not align with the zone of maximum heating power (as in figure 3), but were shifted to the inner part of each heat stripe. Detailed comparison shows that the center of the power strip corresponds nearly with the line separating the dark and shiny region in the visible image, and also near the yellow/orange transition in the IR image (marked with dashed lines). The shiny regions (in the visible) in the heat stripes have an IR emissivity of ~ 0.82 (the same as the original tile material), but the rougher regions (darker in the visible, yellow in the IR) have a higher IR emissivity ~ 0.95 . Far to the sides of the tiles there are regions of deposition, with IR emissivity values climbing to 1.00. Note also the two persistent defect spots on this tile (noted previously in figures 4 and 5), which were present before plasma operation as well. Detailed microscopic tile surface analysis is in progress in Jülich [16].

4. Discussion

We have documented initial infrared observations of W7-X plasma interactions with the limiters used during the first operation of the new W7-X stellarator. High resolution power

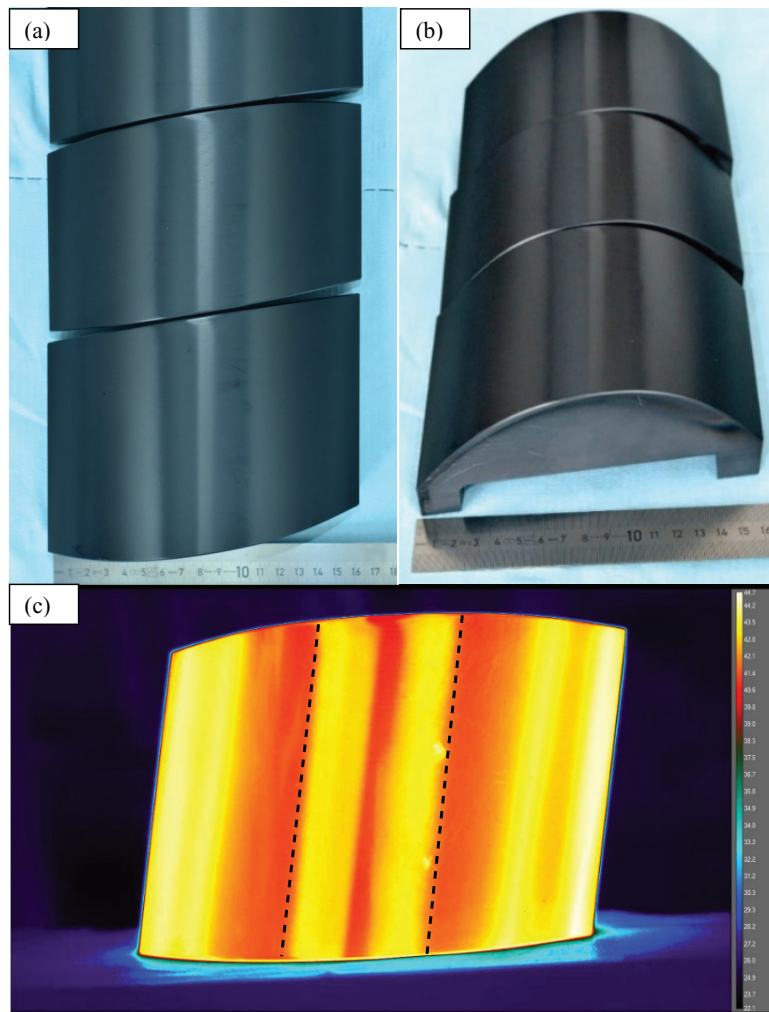


Figure 12. (a) and (b) Post OP1.1 visual close-up of tiles 3, 4 & 5 from Limiter 3. (c) The IR image of Limiter 3, middle tile (#5), in the laboratory at uniform temperature in air, showing fine variations in apparent temperature due to changes in emissivity. IR emissivity values correspond to red ~ 0.82 , yellow ~ 0.95 , and white is 1.00 (movie available in the online version of the paper at stacks.iop.org/NF/57/056036/mmedia).

profile measurements on the limiters were presented, showing heat loads of up to 5 MW m^{-2} , with a complex dual stripe behavior, which depended on the magnetic geometry (two different iota magnetic configurations were used). These agreed well with prior numerical EMC3-EIRENE modeling. By pulling together information from cameras in 3 of the 5 modules of W7-X, and with additional slow thermocouple data from all 5 modules, we were able to estimate the total energy onto the limiters, compared to the ECRH input energy. To do this, we needed to characterize the extent of toroidal and poloidal power load asymmetries. The limiters were precisely designed to define and conform to the plasma shape (in the absence of a limiter), and as evidenced by rather uniform tile-to-tile poloidal (up-down) loading, and they did their job extremely well. The outlier limiter was Limiter 1, in Module 1, which had nearly twice the overall power loads of Limiter 3, and it also exhibited a qualitatively different erosion/deposition pattern on its middle tiles, compared to the other four limiters.

Both the filterscope and FLIR IR cameras saw light fluctuations on the limiter, more pronounced during high power (2 MW or greater) discharges. In terms of IR photons,

these could be 10% of the total flux seen by the IR camera. However the frame-to-frame rate of the IR system (424 Hz maximum for the data that was acquired) wasn't fast enough to follow them, whereas the filterscope did have the necessary bandwidth. We have not ruled out the possibility that the mid-IR camera was, under some conditions, responding to cold dense plasma light transient emission on the limiter surface. The concern is that rotation-vibration bands or even high- n electronic emission from excited molecular hydrogen light (fluorescent molecular light) in the 2.9–5.0 micron wavelength range, could be picked up by the nominal 3–5 micron response of the FLIR camera), rather than it seeing blackbody emission in all cases.

Changes in tile emissivity developed over the course of the campaign, especially in the last few weeks of operation. These coatings caused more than just an emissivity correction on the IR-to-temperature data because they also have different thermal properties than the substrate graphite material, requiring corrections [17] in the THEODOR code on a region-by-region basis over the surface of the limiter. We are still analyzing these 'alpha' corrections for data taken late in the campaign.

5. Conclusion

We have been able to characterize heat fluxes on the poloidal limiters in W7-X during the first helium and hydrogen plasmas during OP1.1. Dual heating stripes with patterns to a large degree matching expectations from the field line geometries. IR thermography and calorimetry using multiple IR camera systems, combined with slow thermocouples to account for toroidal asymmetries, allowed us to estimate that the limiters intercepted up to 60% of the total energy put into the vessel by the ECRH heating system for low power (0.6 MW) long pulse (6s) shots, and a smaller fraction (~35%) for high power (4 MW) short duration (1s) discharges. Local emissivity changes (on the order of 20%) were seen to build up on the graphite limiter tiles during the relatively short operations of OP1.1, and are accounted for in our heat flux estimates. These changes were small for shots during the first half of the run, but the additional thermal property variations due to these coatings are still being analyzed for shots near the end of the run. The high speed, high resolution FLIR IR camera could also see various transients, including dust (UFO's) and higher order energy fluctuations to the limiter.

Acknowledgments

Acknowledgement & Disclaimer: This work has been funded under DOE LANS Contract DE-AC52-06NA25396 and Office of Science grant DE-SC0014210. This work has also been carried out within the framework of the EUROfusion Consortium and has received funding from the H2020 Euratom research and training programme 2014–2018 under grant agreement No 633053. The views and opinions expressed herein do not necessarily reflect those of the European Commission.

References

- [1] Sunn Pedersen T. *et al* 2015 Plans for the first plasma operation of Wendelstein 7-X *Nucl. Fusion* **55** 126001
- [2] Bozhenkov S.A. *et al* 2014 Limiter for the early operation phase of W7-X *41st EPS Conf. on Plasma Physics (Berlin)* P1.080 (<http://ocs.ciemat.es/EPS2014PAP/pdf/P1.080.pdf>)
- [3] Arnoux G. *et al* 2012 A protection system for the JET ITE-like wall based on imaging diagnostics *Rev. Sci. Instrum.* **83** 10D727
- [4] Moulin D. *et al* 2002 The data acquisition system for the infrared cameras on tore supra *IEEE Trans. Nucl. Sci.* **49** 423
- [5] Oh S., Seo D. and KSTAR Team 2011 Optical system design for infrared imaging system of KSTAR *15th Int. Conf. on Laser Aided Plasma Diagnostics (13–19 October 2011)* vol 7 JINST p C02041
- [6] Sieglin B., Faitsch M., Herrmann A., Brucker B., Eich T., Kammerloher L. and Martinov S. 2015 Real time capable infrared thermography for ASDEX Upgrade *Rev. Sci. Instrum.* **86** 113502
- [7] Krychowiak M. *et al* 2016 Overview of diagnostic performance and results for the first operation phase in Wendelstein 7-X *Rev. Sci. Instrum.* **87** 11D304
- [8] Wurden G.A. *et al* 2016 A high resolution IR/visible imaging system for the W7-X Limiter *Rev. Sci. Instrum.* **87** 11D607
- [9] Niemann H. *et al* 2016 Power loads in the limiter phase of Wendelstein 7-X *43rd EPS Conf. on Plasma Physics (Belgium)* P4.005 (<http://ocs.ciemat.es/EPS2016PAP/pdf/P4.005.pdf>)
- [10] Stephey L.A. *et al* 2016 Spectroscopic imaging of limiter heat and particle fluxes and the resulting impurity sources during Wendelstein 7-X startup plasmas *Rev. Sci. Instrum.* **87** 11D606
- [11] Herrmann A., Junker W., Gunther K., Bosch S., Kaufmann M., Neuhauser J., Pautasso G., Richter T. and Schneider R. 1995 Energy flux to the ASDEX upgrade divertor plates determined by thermography and calorimetry *Plasma Phys. Control. Fusion* **37** 17
- [12] Herrmann A. *et al* 1997 Energy deposition at the divertor plates during Elmy H-mode and poloidal and toroidal distribution of heat load on the wall in ASDEX upgrade *Europhysics Conf. Abstracts (Proc. 24th EPS Conf. on Controlled Fusion and Plasma Physics (Berchtesgaden, 1997))* vol 21A pp 1417–20
- [13] Stephey L. 2016 Control of neutral particle fueling and exhaust by plasma edge topology optimization in Wendelstein 7-X and HSX, BAPS *58th Annual Meeting of the APS Division of Plasma Physics* vol 61 JI3.00001 (<http://meeting.aps.org/Meeting/DPP16/Session/JI3.1>)
- [14] Zhang D. *et al* 2016 Investigation of the radiative power loss in the limiter plasmas of W7-X *43rd EPS Conf. on Plasma Physics (Belgium, 2016)* P4.015 (<http://ocs.ciemat.es/EPS2016PAP/pdf/P4.015.pdf>)
- [15] Effenberg F. *et al* 2017 Numerical investigation of edge transport and limiter heat loads in Wendelstein 7-X startup plasmas *Nucl. Fusion* **57** 036021
- [16] Winters V. 2016 Measurement of limiter particle fluxes and carbon erosion in the helical scrape-off layer of startup plasma at W7-X *APS-DPP Meeting (San Jose, CA, 3–8 November 2016)* (http://absimage.aps.org/image/DPP16/MWS_DPP16-2016-001235.pdf) (*Bull. Am. Phys. Soc.* **61** TP10.00073)
- [17] Sieglin B.A. 2014 Experimental investigation of heat transport and divertor loads of fusion plasmas in all metal ASDEX upgrade and JET *PhD Thesis* Technischen Universität of München